AD NUMBER

AD488312

NEW LIMITATION CHANGE

TO

Approved for public release, distribution unlimited

FROM

Distribution authorized to U.S. Gov't. agencies and their contractors; Administrative/Operational Use; JUN 1966. Other requests shall be referred to Commander, AirForce Materials Laboratory, Wright-Patterson AFB, OH 45433.

AUTHORITY

AFSC, USAF ltr, 2 may 1972

THE BOEING COMPANY
Aerospace Group
Space Division

LARGE MOTOR CASE TECHNOLOGY EVALUATION

Contract AF 33(615)-1623

Prepared for

Air Force Materials Laboratory

Wright-Patterson Air Force Base, Ohio

Report
June 1966

I. INTRODUCTION

The purpose of this report is to document the work accomplished on AF 33(615)-1623 since release of the September 1965 Quarterly Progress Report. This work has proceeded at a reduced pace, with emphasis placed on development of 9Ni alloy test data required to help confirm results of the earlier statistical efforts. This resulted in the fabrication and testing of one 9Ni subsize motor case and the testing of several welded fracture and tensile specimens. Specimen and vessel processing followed those procedures dictated by earlier multiple balance and factorial experiments. Additionally, the test vessel contained an artificial crack in the heat affected zone of an intentionally mismatched longitudinal weldment. In effect, this single vessel embodied all major analytical and experimental facets of the alternate materials portion of the program.

II. TEST SPECIMEN PREPARATION AND RESULTS

The 9Ni weldment specimen tests performed during this period consisted of limited tensile, edge notched bend, and surface flawed specimens taken from panels 0.80-inch and 0.50-inch thick. Compositions of base metal and weld-wire are shown in Table I. Plates were heat treated prior to welding, and retempered after welding, as shown in Table II. Weld settings and edge preparation utilized were dictated by the results of the earlier statistical weld development efforts, and were expected to result in near optimum characteristics of properties and quality. Details of weld parameters used are shown in Table II. Weld quality, as determined by visual, penetrant, and radiographic inspection, was acceptable; no cracks were observed, some scattered porosity up to 0.06 diameter was apparent.

Test results of specimens machined from the welded panels are shown in Table III. It is seen that the surface flaw K_{Ic} values average 156 and 149.3 KSI $\sqrt{IN}$ for the 0.80-inch thick weldments with flaws in the weld centerline and in the heat affected zone respectively. Comparative averages from the 0.50-inch plate edge notch specimens are 153.4 and 149.4 KSI $\sqrt{IN}$, respectively. Toughness values from the edge notched specimens were based upon load at the tangent interaction of the load-deflection charts, since pop-in indications from the strain gages bonded near the flaw tip were not observed.

While critical K values are shown for specimens 3 through 9 in Table III, specimens 4 and 6 were actually tested under sustained load conditions. Specimens 4 and 6 were loaded to a target K level of approximately 90% of critical in a 3½% salt spray environment until failure. K_{Ic} values and actual K_{Ii}/K_{Ic} ratios were calculated after failure by measuring the observed flaw growth. Failure times were 8.4 and 15.1 hours respectively for specimens 4 and 6. Actual K_{Ii}/K_{Ic} ratios for the two specimens were .915 and .880 respectively. These data are plotted in Figure 1, along with the band of data developed earlier for 18Ni(200) weldments. The resulting plot shows that the 9Ni weldments appear to be slightly less sensitive to the environment than are the 18Ni(200) weldments. The trend suggests a K threshold value on the order of 85% of critical.

III. 9Ni TEST VESSEL

One 9Ni subscale vessel, with a thickness corresponding to nominal 156-inch case requirements (0.50 inch) was fabricated and tested, utilizing the welding, heat treating, and inspection procedure developed earlier in the program. To simulate potentially severe production circumstances, one of the longitudinal weldments contained an intentional radial mismatch and a simulated surface flaw. Details of design, fabrication, inspection, test, and analysis follow.

A. Vessel Design

The test vessel consisted of a 0.50-inch thick cylindrical section, 18 inches in diameter, and two 0.50-inch spherical hot spun heads. A pressure fitting machined from 2.0-inch plate was welded into one head, the opposite head contained a manual plug weld to fill the 3/4-inch spin mandrel hole. One longitudinal weldment contained a radial mismatch averaging approximately 0.040 inches and a fatigue cracked surface flaw in the heat affected zone of the mismatched weldment. Selection of the amount of mismatch and of the target flaw size was based upon the following:

Utilizing design factors similar to that of the early 623A motor cases (i.e., a 1.3 safety factor, a 1.1 proof factor, and a .95 weld factor) and an assumed minimum yield strength of 170 KSI, comparable operating and proof stresses for the 9Ni alloy would be:

$$\text{Operating stress, } \sigma_{op} = \frac{170 \times .95}{1.3} = 124.2 \text{ KSI}$$

$$\text{Proof stress, } \sigma_p = 1.1 \ \sigma_{op} = 136.6 \text{ KSI}$$

Test pressures, using these stress values would then be:

$$\text{Operating pressure, } P_{op} = 7307$$

$$\text{Proof pressure, } P_p = 8038$$

Now, if it is assumed that in actual production practice maximum design deviations would be controlled to prevent stressing above yield strength at proof pressure, the maximum allowable longitudinal weld radial mismatch can be calculated. Using the results of the stress analysis efforts developed earlier (Reference 1), the maximum total membrane plus extreme fibre stress in a radially mismatched longitudinal joint is:

$$\sigma_{TOTAL} = \frac{P_p R}{t} + \frac{3\delta}{t^2} P_p$$

where P_p = proof pressure = 8038 psig

t = vessel thickness = .50 in.

R = inside radius = 8.50 in.

δ = radial mismatch = unknown

$\sigma_{Total} = \sigma_{yield} = 170$ KSI

Solving for δ, it is seen that the maximum allowable mismatch is 0.04 inches. This would result in a total fibre stress equal to yield strength at proof pressure.

Flaw size dimensions were selected such that the applied K at proof pressure would be equal to the "wet" threshold value of 85% of critical. That is, up to the proof pressure, neither slow growth nor failure would be expected, even in an adverse environment. Using the minimum heat affected zone toughness value of 147 KSI $\sqrt{IN}$ (from Table III), the maximum allowable applied K at proof is .85 x 147 = 124.9 KSI $\sqrt{IN}$. Conservatively assuming that the equivalent gross stress is equal to the membrane plus extreme fiber bending stress, the maximum allowable flaw size, then, is:

$$(a/Q)i = \frac{1}{1.21\,\pi} \left(\frac{124.9}{170}\right)^2 = .142$$

For a three-to-one flaw shape, actual depth and length of the allowable flaw is .21 and .63 respectively.

Using the same assumption regarding equivalent gross stress, and temporarily neglecting yielding effects, the expected burst pressure is conservatively estimated to be:

$$P_{Burst} = P_{proof} \times \frac{K_{Ic}}{K_{Ii} \text{ at } P_{proof}} = 8038 \times \frac{147}{124.9} = 9460 \text{ psi}$$

A less conservative estimate of burst pressure can be calculated by using a solution for a surface flaw in bending developed recently by Smith (Reference 2):

$$K = 1.95 \times \sigma_B (a/Q)^{\frac{1}{2}} Mk$$

where σ_B = bending fibre stress

$Mk = f(a/2c \text{ and } a/t) = .74$

By adding the separate applied K values produced by bending and by the membrane stress, expected burst pressure is 10,070 psig.

While the effects of yielding were neglected earlier in calculating burst pressures, it can be seen that those effects should be minimal in the latter case. For example, at the expected burst of 10,040 psig, the membrane and outside fiber, stresses are 177 and 42 KSI respectively, for a total bending stress of 219 KSI. However, at the bottom of the flaw, the fiber stress is reduced to 8 KSI, giving an equivalent gross stress field of 185 KSI, or 4 percent above typical yield strength.

As a result of the above considerations, the vessel was designed to contain a radial mismatch of 0.04 inches, and an artificial flaw with depth and length targets of .21 x .63 respectively. Expected burst was between 9460 and 10,070 psig.

B. Vessel Fabrication and Inspection

One 18-inch diameter 9Ni vessel was fabricated utilizing procedures similar to that used in the flat test panel tests. Base metal and

weld wire heats, and heat treatment temperature were identical to that of the test panels (see Tables I and II). Because of variation in equipment and part configuration, however, minor weld setting variations were required. These are shown in Table IV.

Radiographic inspection of the girth welds revealed several tungsten inclusions to .090 and scattered porosity, mostly .020 to .060, but up to .120-inch diameter. Two spots with single pores .100 and .120 inch diameter were repaired manually. Radiographic inspection of the longitudinal welds revealed some scattered porosity to .060, but nothing which would require repair.

Prior to testing, the two longitudinal weldments were inspected using automated ultrasonic procedures developed earlier in the program. The procedure included scanning from six positions, three on each side of the weld. The three positions represented three different distances from the weld so that each position inspected a different portion of the weld but with some overlapping of coverage. A 45° shear wave with three bounces, and a standard of a 3/64-inch square slot set to give a saturated signal was used. The transducer was operated at 2.25 mc. Two areas displayed a signal response greater than the 3/64 standard and, though they were not considered rejectable, they were noted for further investigation after burst test.

C. Vessel Test

The vessel test sequence included electrical discharge machining an elliptical notch in the mismatched longitudinal weldment, and extending the notch by pressure cycling as shown in Figure 2. The fatigue extension consisted of 4000 cycles between zero and 2500 psig and 8146 cycles between zero and 3500 psig. After the crack had been initiated

the tank was proof tested to 8040 psig at a pressure rate of 800-900 psig per minute, held for one minute, and reduced to zero pressure. The tank was repressurized to 7300 psig, held for five minutes, simulating a firing cycle, and then pressurized to failure at the same pressure rate as that used in the proof test.

The tank failed at an ultimate pressure of 9840. Overall view of the failed tank is shown in Figure 3. Observation of the vessel indicated that failure initiated in the artificial flaw, the fracture progressing into both heads without fragmenting. All fracture surfaces except just under the flaw exhibited a full shear fracture. Close up views of the flawed area are shown in Figures 4a and 4b. A photomacrograph of the sectioned origin is shown in Figure 4c. It is seen that the fatigue crack extends into the grain coarsened region of the heat affected zone.

As noted earlier, two areas of the longitudinal weldment displayed ultrasonic responses in excess of the 3/64 standard. These were carefully sectioned and examined to determine their nature. Figures 5 and 6 illustrate the results. Figure 5a shows the ultrasonic trace of one of the indications, and Figures 5b and 5c show photomicrographs at 6X and 20X. Similarly, Figure 6 shows the second indication. Both indications are lack of fusion defects. Although the defect depths were only on the order of .02-inches, it is felt from the ultrasonic trace response that they actually have considerable length. Comparison of these indications with the original radiographs was not conclusive.

IV. FABRICATION CONSIDERATIONS

As a result of the multiple balance and process optimization phase, and as

confirmed by the data presented in the preceding discussion, the following represents recommended fabrication procedures for the manufacture of 156-inch class motor cases:

Joint design	Double "U", 0.156" full radius, 40° included angle, .080 root face, 0.00 root opening.
Weld filler	Heat #3888727 or equivalent chemistry
Cleaning procedure	Fresh machined joint surface plus degrease or mechanical cleaning as necessary. Interbead cleaning - wire brush or grinding as necessary.
Weld process	Tungsten inert gas (GTA)
Shielding atmosphere	Argon or helium, preferably helium
Preheat	Preheat is not necessary although in heavy sections it is desirable. The weld interpass temperature should not exceed 300°F or the cooling will be too slow for effective hardening - a good range is 150-250°F.
Machine Settings	Weld machine settings vary from one unit to another, our flat welds were made at 250-275a, 9.5-10V, 5.5-6 ipm, with 20 ipm filler. The tanks were welded at 210-225a, 12-13V, 6 ipm with 24 ipm filler. Differences in machine and heat sink were responsible for the lower heat on the tanks.
Pass Placement	Weld passes should be staggered so as not to have a continuous, coarse dendritic structure at the weld centerline.
Post weld tempering	Contrary to the recommendations of the plate manufacturer and the practice of one fabricator we recommend that the weld be tempered using

the same cycle originally used on the plate but 25°F lower, eg., 2 hrs at 950°F, air cool.

Root pass cracking was encountered early in the program in the 0.8" plate when the penetration was full and the underbead unsupported. This condition was not experienced in 0.5" plate. Based upon conversations with welding representatives of two other firms using this alloy, this phenomonen is not unique to Boeing or to the heats of material under study in this program.

In double "U" joint configurations this problem can be overcome by employing partial penetration on the root pass and, before welding the second side, removing the unfused area by grinding. An alternative method would employ a metal backing bar to support the underbead. It has also been reported that very slow (4-5 ipm) welding speeds on the root pass will reduce the cracking. Neither cracking, other than on the root pass, nor lack of fusion has been a major problem with this alloy. The porosity level appears somewhat greater than other high strength steels but the toughness is sufficiently great that the porosity encountered is tolerable.

REFERENCES:

1. First Year Summary Progress Report on AF 33 (615)-1623.

2. Smith, F. W., "Stresses Near a Semicircular Crack", Ph.D. Thesis, University of Washington, 1966.

C. F. Tiffany
Project Manager

TABLE I

9 Ni COMPOSITION

	HEAT	C	Mn	P	S	Si	Co	Ni	Cr	M_o	V
WELD WIRE	3888727	.22	.30	.006	.005	.26	3.65	7.50	.99	1.02	.07
BASE METAL	3930960	.26	.33	.006	.010	.01	3.9	8.38	.39	.49	.08

TABLE II

9Ni WELD TEST PANEL PROCESSING PARAMETERS

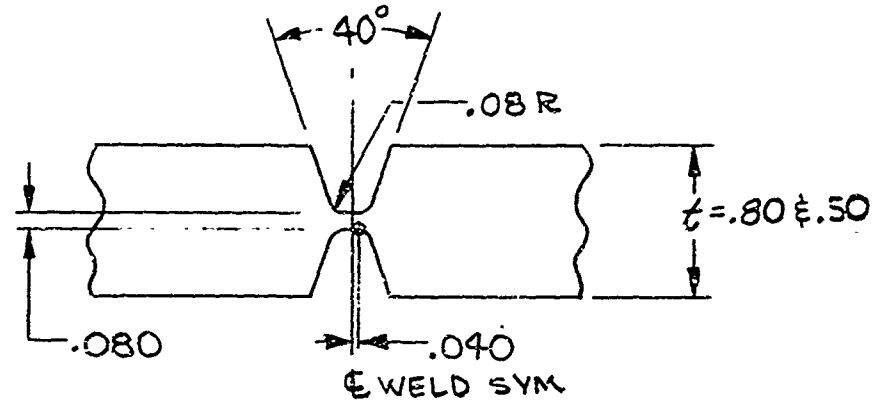

CURRENT	=	275 AMPS
VOLTAGE	=	9.5-10
SPEED	=	5.5-6 IN/MIN
WIRE FEED	=	20 IN/MIN -.062" DIA

HEAT TREAT

BEFORE WELDING – AUSTENITIZE : 1 HOUR AT 1500°F, OIL QUENCH

TEMPER : 2+2 HOURS @ 975°F, AIR COOL

AFTER WELDING – RE-TEMPER : 2 HOURS @ 950°F, AIR COOL

TABLE III

9 Ni DETAILED WELDMENT FRACTURE TESTS

Specimen Number	Gage	Specimen Type	Ult. Strength (ksi)	Yield Strength (ksi)	Net Fracture Stress (ksi)	K_{Ic} ksi$\sqrt{in.}$
1	.80	Tensile	202.2	182.1	-	-
2	.50	Tensile	201.7	178.3	-	-
3	.80	Surface Flaw ℄	-	-	176.2	159.0
4	.80	Surface Flaw ℄	-	-	162.7	153.0
5	.80	Surface Flaw (HAZ)	-	-	165.5	147.8
6	.80	Surface Flaw (HAZ)	-	-	157.8	150.7
7	.50	Edge Notch-Bend ℄	-	-	142.9	154.4 *
8	.50	Edge Notch-Bend ℄	-	-	142.6	152.3 *
9	.50	Edge Notch-Bend (HAZ)		-	137.5	149.4 *

* Value taken at tangent intersection

EDGE-NOTCH BEND

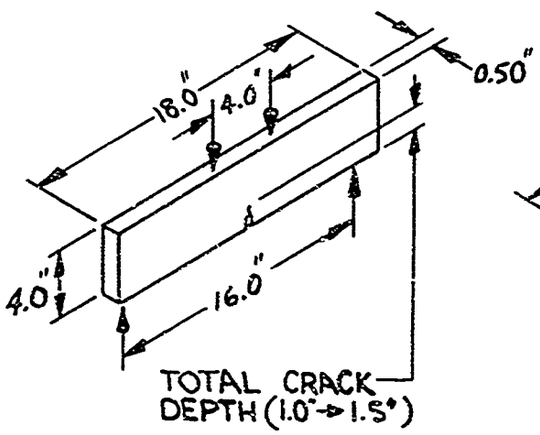

SURFACE FLAW

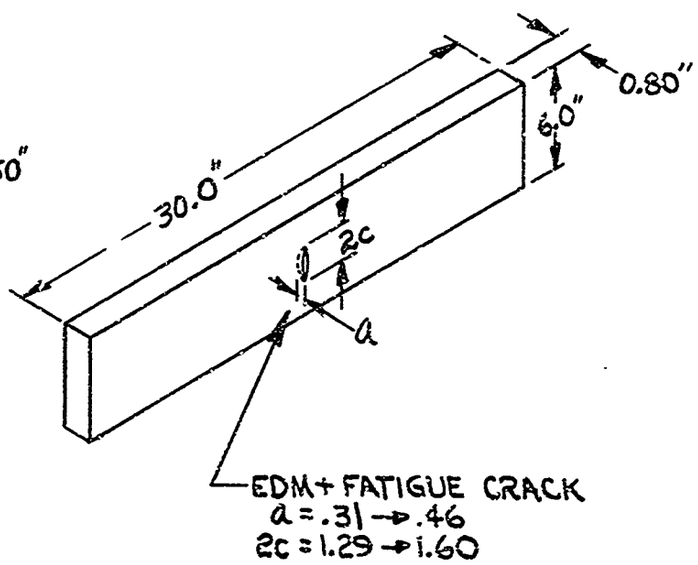

TABLE IV: 9Ni VESSEL WELD PARAMETERS

	GIRTH WELDS		LONGITUDINAL WELDS	
JOINT CONFIGURATION	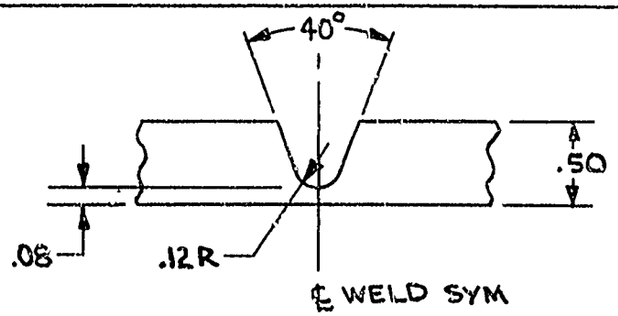		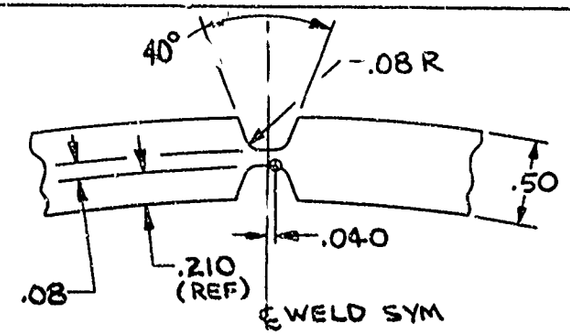	
PASS	1	2 & ON	1	2 & ON
CURRENT	170 AMPS	210 AMPS	190 AMPS	225 AMPS
VOLTAGE	12	12-13	13	13
SPEED	6 IN/MIN	6 IN/MIN	6 IN/MIN	6 IN/MIN
WIRE FEED	24 IN/MIN	24 IN/MIN	22 IN/MIN	22 IN/MIN
SHIELD	He	He		

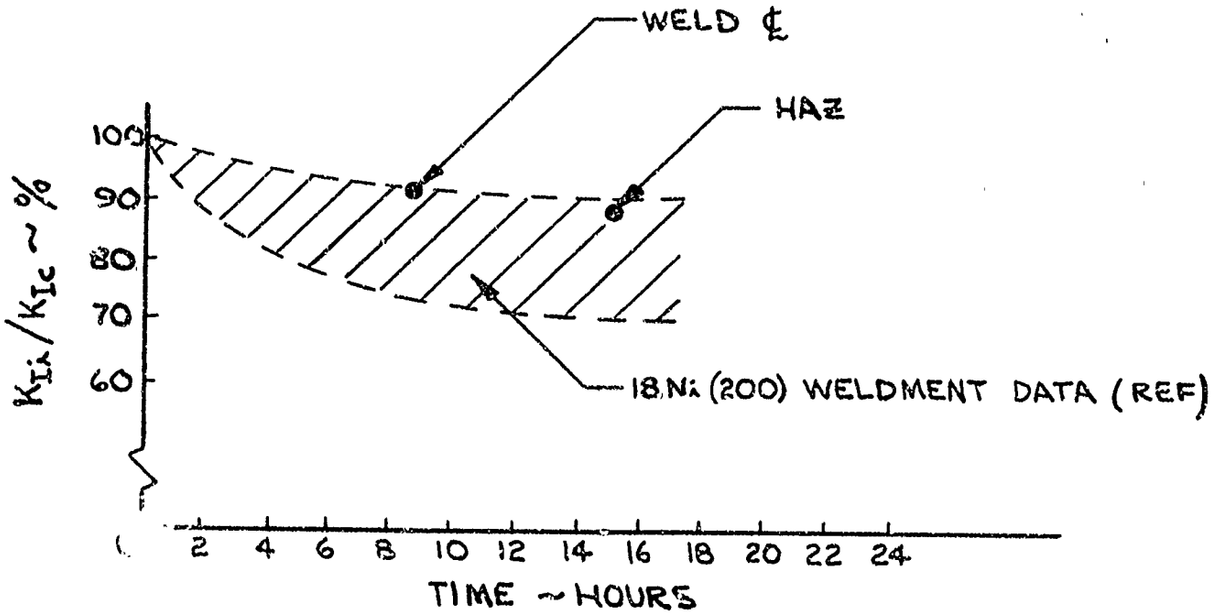

	HEAT NO.
BASE METAL	3930960
WELD WIRE	3888727

Figure 1 : 9Ni WELDMENT SUSTAINED LOAD BEHAVIOR IN 3½% NaCl

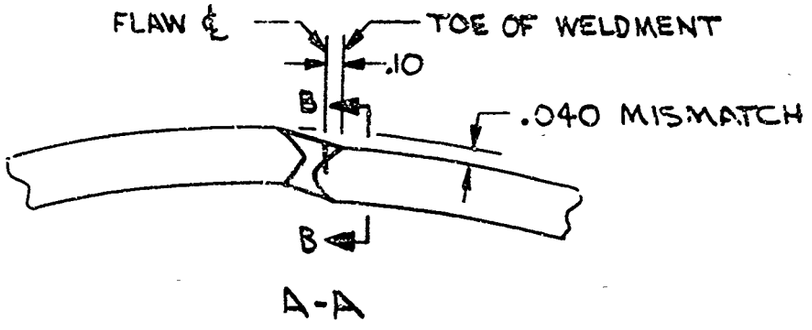

A-A

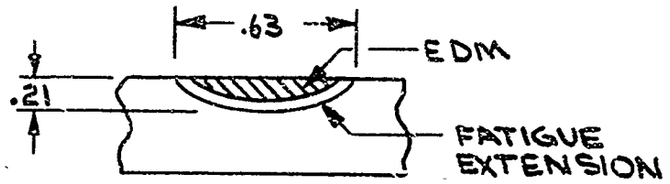

B-B
TARGET FLAW
DIMENSIONS

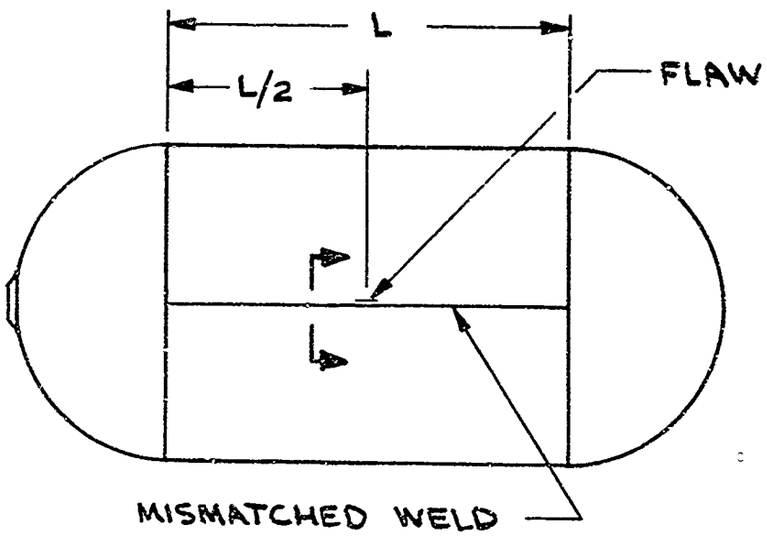

FIG. 2: FLAW AND MISMATCH DETAILS

Figure 3 : OVERALL VIEW OF FAILED 9N; VESSEL

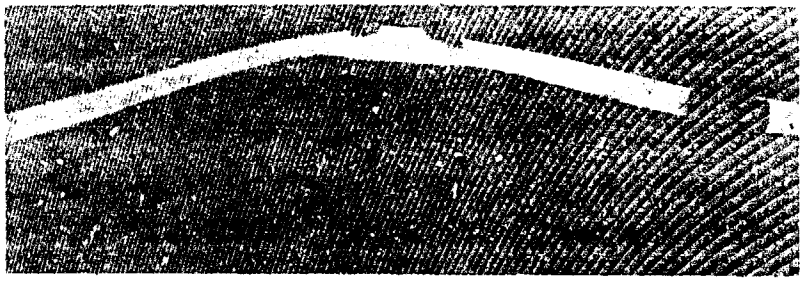

Fig. 4a

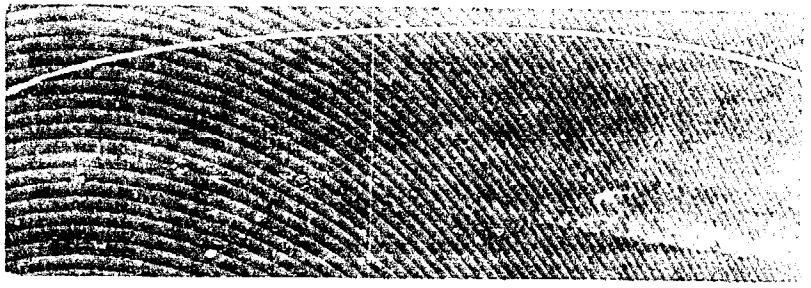

Fig. 4b

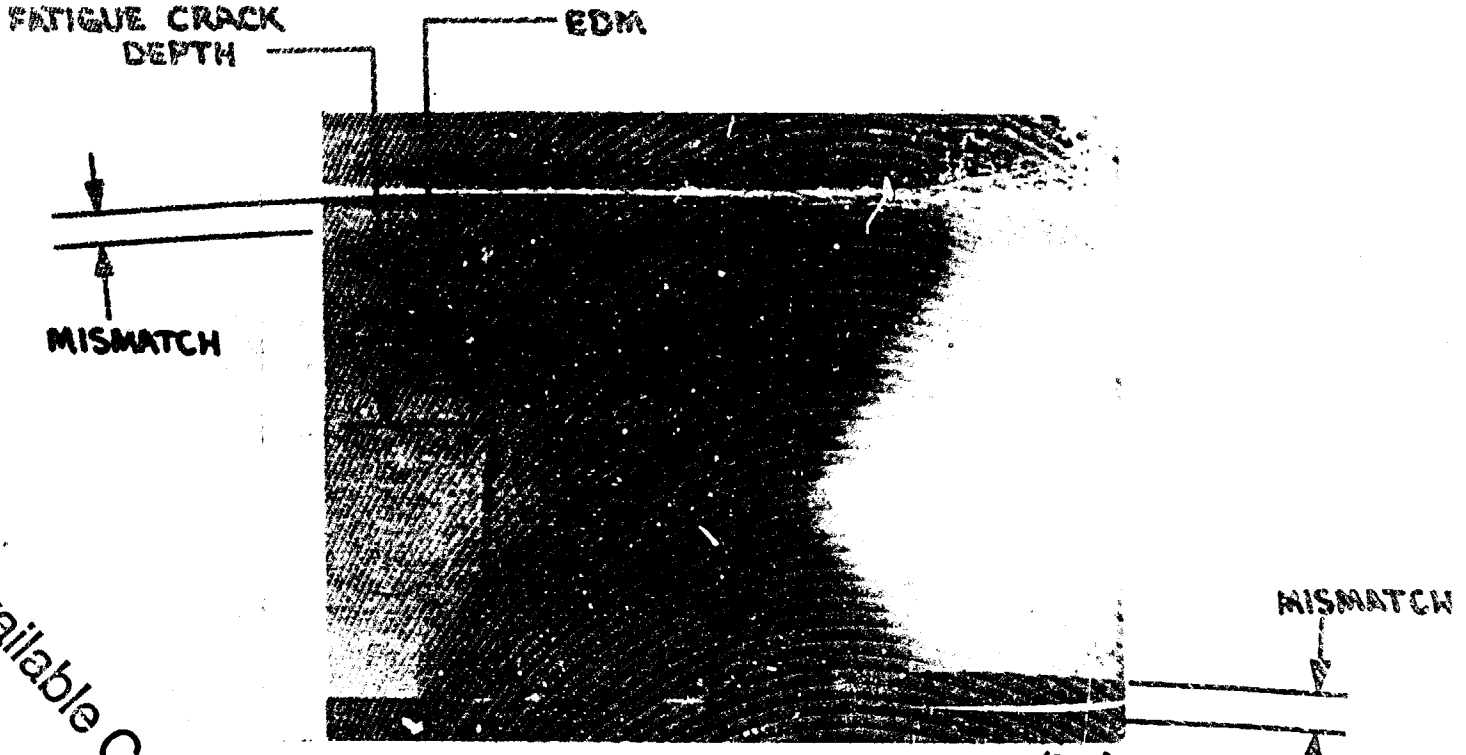

Fig. 4c

Figure 4: FAILURE ORIGIN

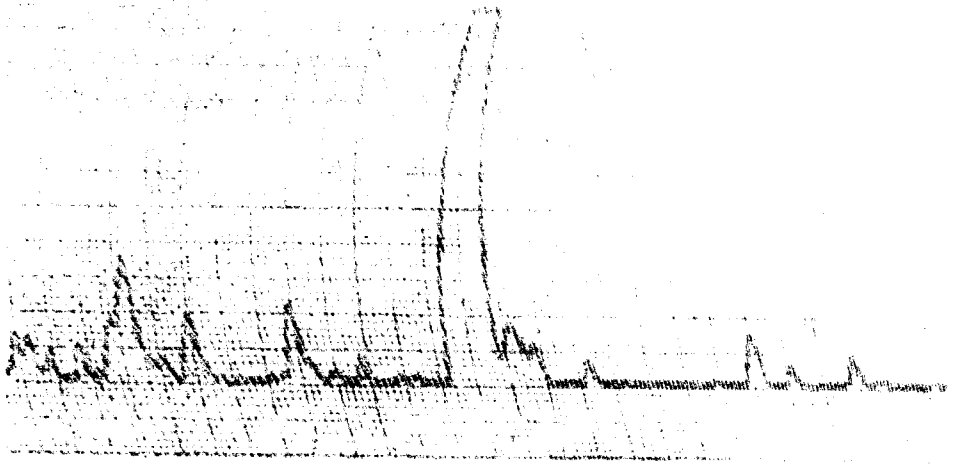

Fig. 5a : ULTRASONIC TRACE

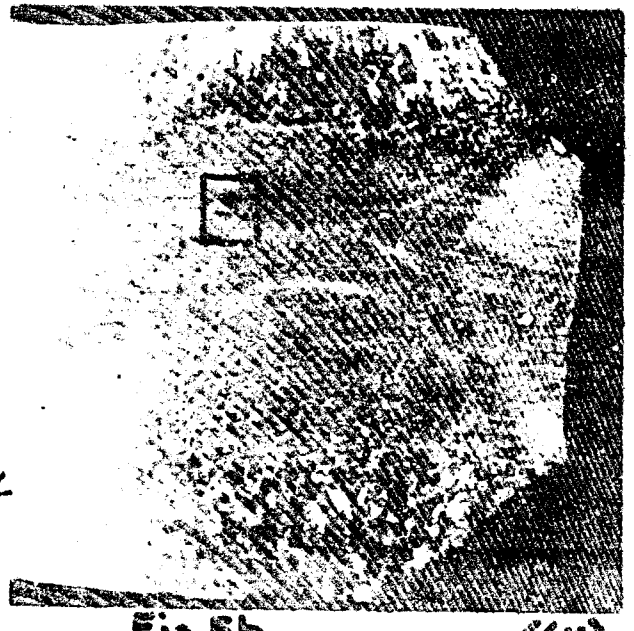

Fig. 5b (6x)

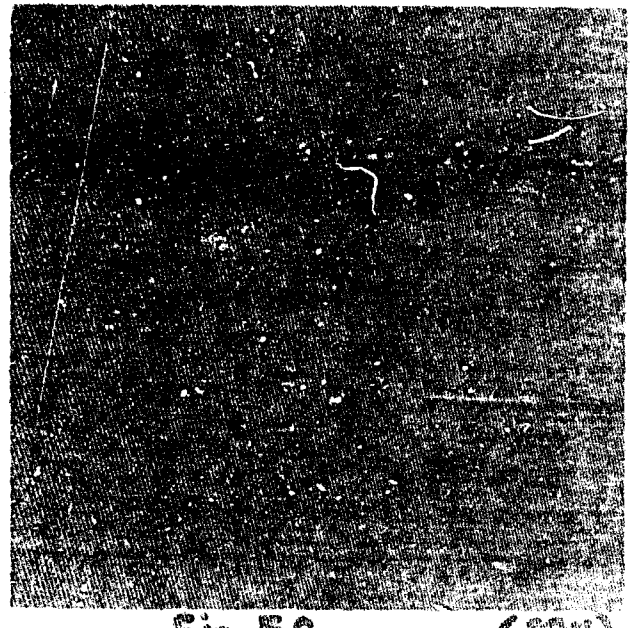

Fig. 5c (80x)

Figure 5 : WELD DEFECT # 1

Fig. 6a: ULTRASONIC TRACE

Fig. 6c (90x)

Fig.6b (9x)

Figure 6: WELD DEFECT #3